Research Article

Journal of Environmental Nanotechnology

Enhancing the Mechanical Properties of Coir Fiber-reinforced Concrete Using Nano-silica

M. K. Muniyasamy[1*], M. Dinesh Kumar[1], Basanth Babu K. Mohanram[2], K. Ramesh[3] and N. Devendran[1]

[1]Department of Civil Engineering, Saveetha School of Engineering, Saveetha Institute of Medical and Technical Sciences, Chennai, TN, India
[2]Department of Civil Engineering, Ultra College of Engineering and Technology, Ultra Nagar, Madurai, TN, India
[3]Department of Civil Engineering, PSNA College of Engineering and Technology, Dindigul, TN, India
Received: 25.01.2025 Accepted: 23.03.2025 Published: 30.03.2025
*munishcivilian@gmail.com

ABSTRACT

Coir fiber (CF) is an economical, eco-friendly, readily processed and easily available natural fiber. The development of strategies to mitigate the detrimental impact of CF on compressive strength (CS) is necessary in order to incorporate it into cementitious composites for structural purposes. Consequently, this study employed nano-silica (NS) as an additive to enhance the production of carbon fiber-reinforced concrete (CFRC) due to its filler properties. To fabricate the CFRC, 0, 2, 4, and 6% of CF and NS by cement weight were incorporated. The durability, microstructure, and novel characteristics of CFRC were investigated. The results indicated that CF reduced the density, uniformity, and CS. Furthermore, it enhanced the interior porous feature of the concrete microstructure. The compressive strength, flexural strength (FS), and split tensile strengths (STS) of the concrete were significantly enhanced by the use of up to 2% NS. The addition of up to 4% CF to the concrete in the absence of any NS resulted in an increase in its STS and FS. The microstructure of the CFRC was enhanced by the incorporation of up to 4% NS by refining and closing the apertures generated by the CF. The mechanical properties of CFRC that included CF and NS were evaluated using multivariable statistical models that demonstrated a remarkable level of precision. These models were highly significant.

Keywords: Concrete; Nano-silica; Compressive strength; Flexural strength; Coir fibers.

1. INTRODUCTION

The construction industry is shifting towards sustainable materials to reduce environmental impact while maintaining durability. Coir fiber (CF), a biodegradable and low-cost natural fiber, has the potential for structural applications. However, it negatively affects concrete's compressive strength. To counteract this, nano-silica (NS) is introduced as a filler to enhance the strength and microstructure of the concrete. Utilizing CF in concrete promotes waste utilization, while NS helps reduce the demand for cement and carbon emissions. Sustainable concrete is made from recycled materials such as silica fume, fly ash, and blast furnace slag instead of traditional Portland cement. The inclusion of coir, steel, and polypropylene have shown to enhance mechanical characteristics and diminish plastic shrinkage by as much as 40%. The integration of supplemental cementitious materials (SCMs) and fibers improves durability while promoting eco-friendly concrete (James and John, 2024). Additionally, thermal and mechanical properties of foam concrete can be enhanced by the integration of phase change material, expanded vermiculite, nano-silica, and coir fiber (Dora *et al.* 2023). Waste utilization in concrete for sustainable construction was studied by Senguttuvan *et al.* (2024). It was noted that addition of coir fibers (0.2%–1.2%) improved strength, water absorption, and durability, with optimal results at 0.6% dosage.

Predictive formulas were developed for compressive strength, confirming the effectiveness of fiber reinforcement in expanded-clay fiber concrete (Özkılıç' *et al.* 2023). The concrete paving blocks (CPB) made with mixed reused aggregates from construction and demolition waste (CDW) and coconut fibers. Experimental results show that CPB with CDW and coconut fibers exhibited improved physical and mechanical properties. The study confirms their suitability for use in road pavements for light vehicles (Brasil *et al.* 2024).

The study evaluates high-strength concrete (M70) reinforced with banana and coir fibers, combined with 15% Alccofine. Testing on reinforced concrete beams shows increased load-carrying capacity, with banana and coir fibers enhancing strength by 42.86% and 35.71%, respectively. The results confirm the effectiveness of fiber reinforcement in structural applications (Rajkohila *et al.* 2024). Samson *et al.* (2024) explored steel slag as a granite replacement in concrete, combined with coconut fibers for reinforcement. Enhanced impact resistance and sulfate attack resistance suggested this combination is a viable sustainable alternative. The chemical treatment of coir fiber elevated cellulose content to 49.15%, with an average fiber dimension of 1521 µm. Microstructural investigation by Rahmawati *et al*. (2023) validated the synthesis of C-S-H gels resulting from the interaction of silica from waste glass with cement. The results indicated that waste glass and CF augment mortar strength by enhancing adhesion and crack resistance. Menon *et al*. (2021) conducted laboratory tests on encased stone columns reinforced with CF-based geocell mattresses and crumb rubber to assess soil stabilization. A 10% replacement of stone aggregate with crumb rubber improved the load-settlement response (15%) and interface friction. Bothiraj *et al*. (2022) developed hybrid epoxy composites using waste marble dust (4-16 wt%) as filler and coconut fibers as reinforcement. The experiments showed that 12 wt% marble dust + 16 wt% coconut fiber provided the best mechanical properties.

Fiber-reinforced pavement quality concrete (PQC) was developed using 25% coarse recycled aggregate (CRA) and 1% coir fiber. M35 PQC maintained compressive and tensile strength while increasing bond strength by 45% compared to conventional concrete. These results demonstrate the effectiveness of CRA and coir fiber in PQC applications (Poongodi *et al*. 2022). Coconut fiber-reinforced self-compacting concrete was tested with 0.2%, 0.4%, and 0.6% fiber content. The 0.2% fiber mix achieved the highest compressive and flexural strength while maintaining SCC standards (Odeyemi *et al*. 2023). Coir fiber was incorporated into rendering mortars using cement and air-lime binders at 10% and 20% fiber volume fractions with fiber lengths of 1.5 cm and 3.0 cm. The addition reduced workability and compressive strength but improved flexural strength and fracture toughness (Pederneiras *et al*. 2021). Coir fiber and recycled aggregates were incorporated into cement-bound granular combinations for pavement base layers. Addition of CF reduced mass loss by 42% in wetting-drying tests and 20% in freezing-thawing tests, improving durability and toughness (Crucho *et al*. 2022). Concrete mixes with 50% and 100% recycled aggregates and 2% CF were tested with and without superplasticizer (SP). Coir fiber improved shear strength by 40% with SP and 60% without SP. Chloride permeability and water absorption increased with CF alone but were controlled with SP addition (Ali *et al*. 2022). Sharma and Senthil, (2022) reviewed the impact performance of waste materials in concrete. The 2% coir fiber (40 mm length) showed the highest impact energy absorption and residual strength. Rubber particles up to 15% replacement of coarse aggregate were recommended for impact-resistant concrete.

Foamed concrete was reinforced with 0.3% coir fiber (by cement weight) and 5-8% vermiculite as fine aggregate replacement. Coir fibers enhanced load transfer and minimized shrinkage cracks, making the material more durable (Padmakumar and Madhavan, 2023). Balreddy *et al*. (2023) studied open-graded bituminous concrete (OGBC) with sisal, jute, coir, and bamboo fibers at 0.15%, 0.3%, and 0.45% by mix weight. Fiber addition reduced binder drain down and air voids while improving moisture resistance and tensile strength. Optimal fiber content was 0.30% for sisal, bamboo, and coir and 0.45% for jute.

The present study introduces a novel, eco-friendly approach to enhancing coir fiber-reinforced concrete by incorporating nano-silica to counteract the adverse effects of coir fiber on strength and porosity. Unlike conventional treatments, NS acts as a cost-effective filler, improving mechanical properties while promoting sustainability. By utilizing coir fiber, an agricultural byproduct, and NS, this research reduces construction waste, lowers reliance on synthetic materials, and enhances concrete durability, contributing to a reduced carbon footprint and more sustainable building practices.

Table 1. Chemical composition of Type 1 cement (Waqar *et al.* 2023)

Chemical Composition	Cement (%)
Alumina (Al_2O_3)	4.00
Sodium Oxide (Na_2O)	0.10
Silicon dioxide (SiO_2)	23.00
Sulphur trioxide (SO_3)	2.00
Calcium oxide (CaO)	64.00
Iron oxide (Fe_2O_3)	2.00
Magnesium oxide (MgO)	2.00
Potassium oxide (K_2O)	1.00
Chemical Composition	Cement (%)

Table 2. Physical and chemical properties of coir fiber (Zhang *et al.* 2021)

Parameters	Values
Cellulose (wt%)	36.6
Hemicellulose (wt%)	37.0
Lignin (wt%)	22.2
Average Length (mm)	15
Specific Densities (Kg/m^3)	1540.6
Average Diameter (µm)	250
Bulk Density (Kg/m^3)	69.8
Average Tensile Strength (MPa)	400

2. EXPERIMENTAL METHODOLOGY

2.1 Material

Table 1 lists the chemical composition of Type I cement in compliance with ASTM C150/150M standards. The cement has a bulk density of 1,440 kg/m^3

and a specific gravity of 3.16. A grinder was used to reduce the particle size to less than 38 µm and then the granulated silica was milled. Once the silica was ground into a powder, it was sieved through a 37 µm (No. 400) screen. Additional dry milling was applied to the ground silica to attain nanoscale dimensions. A planetary ball mill called the Pulverisette 7 Premium was used for the milling process. The specific surface area of NS is 3,000 m^2/g, its mean pore width is 2.14 nm, and its bulk density is 0.5 g/cm^3.

The fine aggregate was composed of natural river sand that was both dust-free and pristine. The fine aggregate had a bulk density of 1,565 kg/m^3, a specific gravity of 2.63, and a fineness modulus of 2.26. Additionally, the aggregate exhibited a soil content of 1.1% and a water absorption of 1.87%. The gradation curve of the fine aggregate is depicted in Fig. 1, which is consistent with the ASTM C33 specification. The coarse aggregate was composed of crushed granite. In order to eradicate any impurities and particles, the aggregate was meticulously rinsed with purified water. The aggregate had a bulk density of 1,462 kg/m^3, a specific gravity of 2.71, and a maximal nominal size of 19 mm.

Coir fiber was acquired from fiber source firms located in Chennai, Tamil Nadu. The fibers were immersed in clean water and carefully cleaned. In order to eliminate all contaminants and impurities, the purified fibers were submerged in a 3% NaOH solution for approximately three hours. Subsequently, the fiber mesh was thoroughly cleansed with purified water to guarantee that the fibers-maintained diameters of 1.2 to 1 mm and lengths of 25 to 35 mm. Before being incorporated into the concrete, the individual filaments were permitted to air dry completely for approximately 48 hours. Table 2 illustrates the characteristics of the CF.

2.2 Mixture Ratio

The constituent ingredients of the control mix were determined and the concrete was designed using the ACI 211.1R methodology. In order to reduce the influence of variations in the water-to-cement ratio among the mixtures, the superplasticizer volume was maintained at 1% (by weight). The CF was incorporated into the composites at varying concentrations (2%, 4%, and 6% by weight) of the binder. The NS was incorporated into the CFRC at 2%, 4%, and 6% (by cement weight) as an additive. As illustrated in Table 3, 16 composites were generated from a variety of CF and NS combinations, including the control.

Table 3: Composition of mixture ratio for composite samples

Sample Number	Quantities for 1 kg/m^3						
	Fine aggregate	Coarse aggregate	H_2O	Superplasticizer	Cement	CF	NS
Control	700	880	175	5.5	490	0	0
S1	700	880	175	5.5	490	0	0
S2	700	880	175	5.5	490	9.8	0
S3	700	880	175	5.5	490	19.6	0
S4	700	880	175	5.5	490	29.4	0
S5	700	880	175	5.5	490	9.8	9.8
S6	700	880	175	5.5	490	19.6	9.8
S7	700	880	175	5.5	490	29.4	9.8
S8	700	880	175	5.5	490	0	19.6
S9	700	880	175	5.5	490	9.8	19.6
S10	700	880	175	5.5	490	19.6	19.6
S11	700	880	175	5.5	490	29.4	19.6
S12	700	880	175	5.5	490	0	29.4
S13	700	880	175	5.5	490	9.8	29.4
S14	700	880	175	5.5	490	19.6	29.4
S15	700	880	175	5.5	490	29.4	29.4

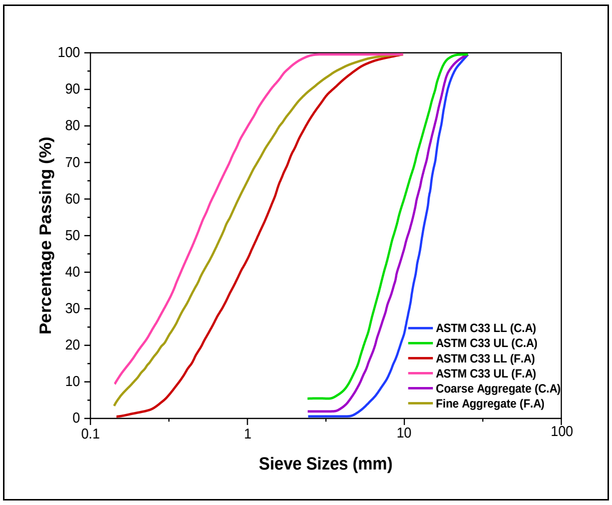

Fig. 1: Gradations of aggregate particle sizes

Fig. 2: Fabrication of hardened samples

Fig. 3: Pictorial representation of samples placed in compression testing machine

2.3 Fabrication of Samples

In order to evaluate the formulated combination proportions, they were generated in the laboratory. The constituent elements of the mix were all weighed. The methods outlined in ASTM C192/C192M were followed during batching, blending, and casting the concrete samples. To stop the aggregates from absorbing some of the mixing water, they were soaked and surface-dried before combining. The cement was free from agglomeration, impurities, and foreign particles.

After adding the cement, NS, and fine aggregate to the mixer, the mixture was vigorously stirred for about 45 seconds. The superplasticizer and CF were incorporated incrementally during the mixing process. The superplasticizer, residual water, and coarse aggregate were incorporated. The process of mixing continued until a completely homogeneous mixture was attained. As soon as the concrete was mixed, its fresh density and sinking were measured. The freshly mixed concrete was then poured into the appropriate molds and left in the lab for a full day to cure and consolidate. They were taken out of the molds once they had solidified and allowed to cure in clear water (Fig. 2).

2.4 Testing methodology

To evaluate the workability of new concrete following casting, the slump test was carried out in compliance with ASTM C143/C143M requirements. Following that, the revised density was evaluated using the guidelines provided in ASTM C138/C138M.

The compressive strength was assessed after 14 and 28 days of curing to assess the toughened characteristics. The BS EN 123903 standards were followed in the manufacturing and testing of 100 mm^3 samples. Fig. 3 illustrates the compression testing machine with a 1500 kN capacity. The same testing machine was used to measure split tensile strength. Cylindrical specimens with 110 mm diameter and 210 mm height were fabricated and cured for two different periods (14 and 28 days) before testing. According to the procedures described in BS EN 12390-6, the tensile strength test was carried out. The ASTM C78/C78M procedures were followed when performing the flexural strength test. Before testing, raw specimens with dimensions of 110 mm width, 110 mm height, and 510 mm length were fabricated and cured in water for 14 and 28 days. The ASTM C78/C78M procedures were followed for conducting the water absorption test. Prior to testing, 100 mm^3 specimens were made and allowed to rest for 4 weeks. The samples were dried for one day at 100℃ prior to testing. After drying the samples, they were placed in pure water for one more day and weighed. Following immersion in water, the samples were weighed again. Water absorption was determined using the two reported weights.

The chosen samples were subjected to microstructural analysis. A field emission scanning electron microscope was used to examine the CFRC's microstructural morphology. Concrete samples were taken out after 28 days of curation. Before applying a thin layer of gold, the sample was thoroughly dried to remove moisture and cleaned to eliminate any impurities. The morphology of coated samples at various magnifications and resolutions was recorded using a high-resolution computing system and subsequently inserted into the FESEM. A subset of samples underwent X-ray diffraction (XRD) examination to evaluate the changes in the CFRC's structure, crystallinity, and chemical composition brought about by the addition of NS. The standard formulations were left to cure for 28 days before the paste samples were extruded. The pastes were subsequently desiccated and purified, and they were subsequently ground into a fine NS. The specimen was subsequently incorporated into the apparatus, and the high-resolution computer system connected to the device was used to acquire the results.

2.5 Analysis through Multi–criteria Decision Making (MCDM)

2.5.1. Method based on the Removal Effects of Criteria (MEREC) Method

The performance of composite materials was assessed and rated by MCDM analysis taking into account various conflicting criteria. The essential criteria including compressive strength (CS), flexural strength (FS), tensile strength (TS), wear resistance, density, and water absorption were selected due to their significance to the material's mechanical and tribological properties. A decision matrix was created utilizing the experimental data, and normalization methods such as Min-Max or Vector normalization were employed to guarantee comparability. Criteria weights were allocated utilizing approaches such as MEREC and ARAS to rank the composite formulations.

Step 1: In this step, a decision matrix showing each alternative's scores or values with respect to each criterion was created. The elements, denoted by X_{ij}, must be larger than zero (positive values). Accordingly, a decision matrix was developed.

$$X = \begin{bmatrix} x_{11} & x_{12} & \cdots & x_{1j} & \cdots & x_{1m} \\ x_{21} & x_{22} & \cdots & x_{2j} & \cdots & x_{2m} \\ \vdots & \vdots & \ddots & \vdots & \ddots & \vdots \\ x_{i1} & x_{i2} & \cdots & x_{ij} & \cdots & x_{im} \\ \vdots & \vdots & \ddots & \vdots & \ddots & \vdots \\ x_{n1} & x_{n2} & \cdots & x_{nj} & \cdots & x_{nm} \end{bmatrix} \quad \ldots (1)$$

Step 2: The decision matrix was normalized according to Equation (2) for both advantageous and non-beneficial criteria.

$$n_{ij}^{x} = \begin{cases} \dfrac{\min_k x_{kj}}{x_{ij}} & \text{if} \quad j \in \mathcal{B} \\ \dfrac{x_{ij}}{\max_k x_{kj}} & \text{if} \quad j \in NB \end{cases} \quad \ldots (2)$$

Step 3: The cumulative performance of the response, denoted as k_i, was computed.

$$k_i = \ln\left(1 + \left(\frac{1}{m}\sum_j \left|\ln\left(b_{ij}^{*}\right)\right|\right)\right) \quad \ldots (3)$$

Step 4: The performances of alternatives, (k_{ij}^{*}) were quantified by eliminating each criterion (Sathishkumar *et al.* 2024).

$$k_{ij}^{*} = \ln\left(1 + \left(\frac{1}{m}\sum_{k,k\neq 1} \left|\ln\left(b_{ij}^{*}\right)\right|\right)\right) \quad \ldots (4)$$

Step 5: In Equation (5), the total absolute deviations, (A_j) were ascertained.

$$A_j = \sum_i \left|k_{ij}^{*} - k_i\right| \quad \ldots (5)$$

Step 6: The weightage of the criterion was determined using Equation (6) (w_{jMEREC}).

$$w_{jMEREC} = \frac{A_j}{\sum_K A_k} \quad \ldots (6)$$

2.5.2. ARAS Techniques

Step 1: Equation 1 was is employed to generate a decision matrix.

Step 2: A normalization value for both beneficial and non-beneficial criteria was obtained.

Equation (7) was employed to compute the normalized matrix for the beneficial criteria.

$$N_{ij(\text{benificiary})} = \frac{(T_{ij})}{\sum_{i=1}^{k} T_{ij}} \quad \ldots (7)$$

The TS and hardness of the beneficiary criteria were calculated using their normalized values.

Step 3: Equation (8) was been used to calculate the normalization matrix for the non-beneficial criteria (Gupta *et al*. 2024).

$$\check{T}_{ij} = \frac{1}{T_{ij(\text{ nonbenificiary})}}, N_{ij(\text{ non benificiary}} = \frac{(T_{ij})}{\sum_{i=1}^{k} T_{ij}} \ldots (8)$$

The normalization values of non-beneficial criterion, such as tool wear loss, were also computed.

Step 4: Calculation of the weightage normalization matrix

The benefit criterion was assigned a weight of 0.3 in order to improve both microhardness and tensile strength. Weight assigned to the reduction of tool attrition rate was 0.4, which was anticipated to increase the longevity of the tool. Equation (9) delineated the equation for evaluating a weightage normalization matrix.

$$WN_{ij} = W_j \times N_{ij} \quad \ldots (9)$$

where, W_j - weight to the j^{th} criteria.

Step 5: Finding the optimality function for every possible solution

Each alternative solution's optimality function was determined using the following equation.

$$OF_i = \sum_{j=1}^{1} WN_{ij}, i = 1,2 \ldots, k \qquad \ldots (10)$$

Equation (11) was used to ascertain the optimal value for all alternative solutions.

$$OF_o = \max OF_i \qquad \ldots (11)$$

Step 6: Evaluation of the utility degree

Using the S_i and S_0 values, the utility degree was determined (equation (12)).

$$UF_i = \frac{OF_i}{OF_o} \qquad \ldots (12)$$

Step 7: Utility degree ranking

The utility degree was ranked in order to determine the most effective and least effective alternative solutions.

3. RESULTS AND DISCUSSION

Fig. 4 depicts the results of slump test for CFRC. The slump values for all mixtures vary from 84 mm to 50 mm. The incorporation of NS resulted in a reduction of slump in the concrete. The slump measurements for S4, S8, and S12 were 82 mm, 65 mm, and 55 mm, respectively, all of which are lower than that of the control (86 mm). The reduction in slump values upon NS incorporation was attributable to its greater surface area, which facilitates increased water absorption to create a uniform paste, hence diminishing workability.

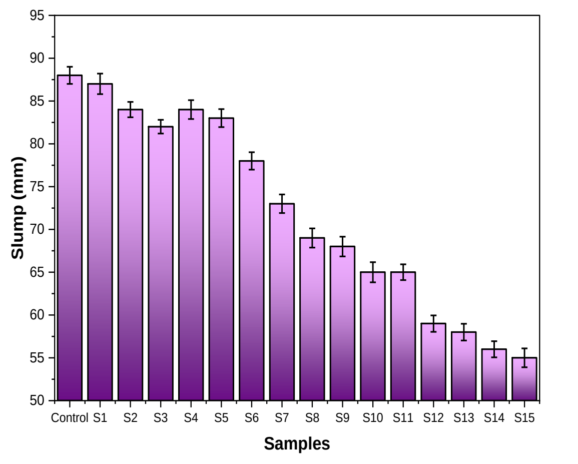

Fig. 4: Slump test results

The incorporation of CF into mixtures with varying ratios of NS led to a further reduction in slump values, as observed in our experimental investigations. The slump measurements for S5, S6, and S7 were recorded as 83 mm, 78 mm, and 73 mm, respectively, compared to 84 mm for S4. Fig. 4 illustrates that the control mix exhibited the highest slump at 88 mm, while the mix containing 6% CF and 6% NS (S15) had the lowest slump at 55 mm. These results confirm that the combined addition of CF and NS reduces the workability of the mix. To counteract this reduction in mix consistency, an increased dosage of water-reducing admixtures such as SP could be considered in future studies to maintain desired workability.

3.1 Density

Fig. 5 displays the density of fresh and hardened mixes. The concrete density marginally augmented with incorporation of upto 4% NS. The fresh density of S4 and S8 exceeded the control by 2.23 and 3.00%, respectively. Similar tendencies in results are observable for density of hardened mixture as well. The density rise is attributed to NS acting as a filler material in the mixture due to its extensive surface area, compacting the fresh mix and enhancing density.

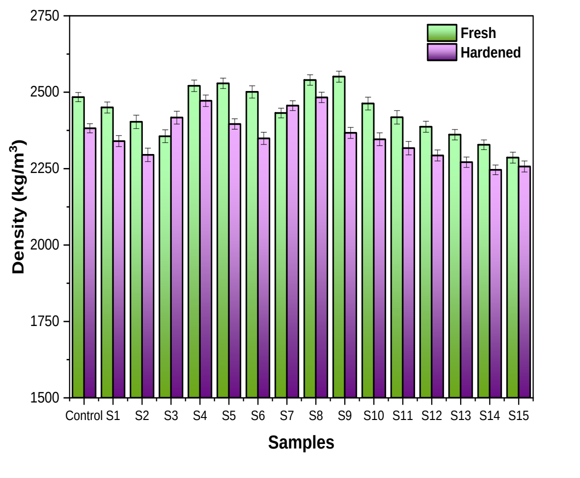

Fig. 5: Density of fresh and hardened mixes

The incorporation of 6% NS resulted in a decrease in the density of both concrete mixtures, likely attributable to a significant decline in uniformity, which led the concentration of NS, leading to air entrainment and drop in density. The inclusion of up to 4% CF in concrete mixtures containing up to 4% NS resulted in an enhancement of the density of hardened and fresh mixes. In mixtures containing 2% NS relative to control mix, the fresh densities of S4, S5, and S6 increased by 2.23, 3, and 1.42%, respectively. A similar trend in results is evident for the hardened mixture. Similarly, mixtures with 2% NS exhibit a greater fresh density than the control mix, showing increases of 3.00, 3.45, and 0.12 % for mixtures S8, S9, and S10, respectively. Moreover, the nano-silica, owing to its smaller particle size, occupies the voids generated by the carbon fiber inside the cement matrix, enhancing the density of the paste. The incorporation of CF into the concrete mixtures with 6% NS resulted in a reduction of fresh densities. The fresh density of samples containing 6% NS, specifically S12, S13, S14, and S15, was reduced by 4.46, 4.26, 5.60, and 7.30% in comparison to the control. The reduction in density may result from the inadequate consistency of the mixture, leading to the concentration of NS and balling effects of CF, which entrain significant amounts of fresh mix air, thus reducing density.

3.2 Analysis of Compressive strength

Fig. 6 illustrates the CS of the CFRC. The CS diminishes as the fraction of CF included increases. At 14 days, the CS of S1, S2, and S3 were reduced by 5.75, 9.49, and 25.12% compared to the control mix. At 4 weeks, the CS of S1, S2, and S3 are diminished by approximately 4.67, 8.24, and 21.74%, respectively, in comparison to control mix. The reduction in CS resulted from hydrophilic characteristics of the CF, which absorbed a part of mixing water, diminishing uniformity of the mixture. It resulted in the development of porosity inside the composite matrix, ultimately causing premature failure and strength reduction. Experimental results show improved compressive, tensile, and flexural strength, attributed to enhanced bonding and a denser mix. The findings highlight the effectiveness of natural fibers in sustainable concrete (Kandasamy *et al*. 2024).

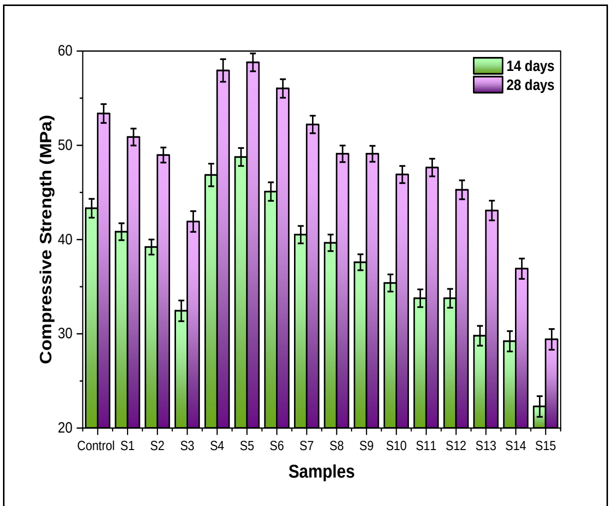

Fig. 6: Compressive strength results

The incorporation of NS into CFRC enhanced its CS. In the 0% CF mixture, the incorporation of 2% NS increased the CS, with the S4 mix showing gains of 5.75%, and 4.67% at 14 and 28 days, respectively, compared to the control mixes. Additionally, the inclusion of 2% NS effectively mitigated the reduction in compressive strength when 2% and 4% CF were included in the mixtures. The compressive strength of S5 mix outperformed the control mix by 12.56, and 10.17% and the S6 mix exhibited increase of 4.09, and 4.98% at 14 and 28 days, respectively.

The incorporation of more than 2% NS into the concrete, regardless of the presence of CF, led to a reduction in CS. In mixes devoid of CF, the CS of S8 was reduced by 8.47, and 8.00% at 14 and 28 days in comparison of control mixes. Similarly, the CS of the S12 was diminished by 22.05, and 15.16% at 14 and 28 days, in comparison of control mixes. The reduction in CS results from disruption of tricalcium aluminate hydration, which is diminished by hydrolysis and ettringite production due to the retarding influence of carbon. Moreover, smaller particle sizes of nano-silica result in the absorption of a part of fraternizing water, therefore making new concrete less effective. It resulted in fiber balling and inadequate compaction, hence augmenting the pore volume within microstructure of the cured concrete. This generates numerous vulnerable pathways for early failure under load applications, resulting in diminished CS. Likewise, coconut fibers (15 mm) helped counteract mechanical property losses, maintaining a compressive strength above 10 MPa. Lightweight recycled brick aggregate concrete showed durability under harsh conditions, making it a viable eco-friendly masonry material (Hameed *et al*. 2025).

3.3 Analysis of Flexural strength

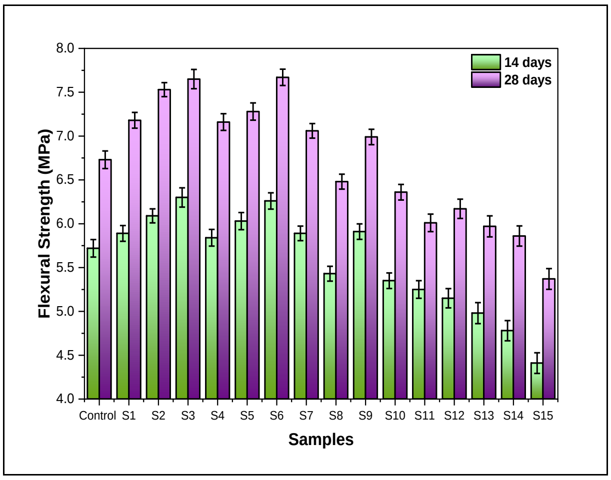

Fig. 7: Flexural strength results

Fig. 7 illustrates the FS of CFRC generated with varying ratios of CF and NS. It was noted that the FS increased with the rise in number of fibers. Relative to its corresponding control mixes, the FS of S1 increased by 2.97 and 6.69% at 2 and 4 weeks and for S2, the enhancement was 6.47 and 11.89% at the same intervals; for S3, the improvement was 10.14 and 13.67% respectively. Similarly, a 3% fiber addition enhanced cumulative heat development in calcium sulfoaluminate cement within 24 hours and 2% coconut fiber improved mortar flexural strength by 16.7%, optimizing mechanical properties (Bui *et al*. 2022).

The incorporation of 2% NS into the mixes devoid of CF augmented its flexural strength, with mix S4 exhibiting enhancements of 2.10 and 6.36% at 14 and 28 days in comparison to the control. The use of 2% NS considerably improved the FS of the CFRC having 2%, 4%, and 6% fibers. This is evidenced by comparing the FS of mixes S5, S6, and S7 with control or corresponding blends S1, S2, and S3. The FS of S5 increased by 5.42% and 8.17% at 14 and 28 days in comparison of control mix. Comparable outcome patterns are seen for mixes S6 and S7. The incorporation of 2% NS only improved the FS of 2% CF. A comparison of the FS of S9 with the control reveals that the former exhibits a superior strength of 3.32 and 3.86% at 14 and 28 days in relation to the latter. The enhancement may result from the synergistic effects of the fiber's crack-bridging capability and the pore-filling properties of the nanoparticles. The incorporation of 4% NS into CFRC with 4% and 6% CF led to reduction in FS, as illustrated in Fig 7. Moreover, incorporation of 6% NS into CFRC with 2%, 4%, and 6% CF resulted in a reduction of FS. Among all the mixes, the concrete containing 6% CF and 6% NS (S15) exhibits the lowest flexural strength, with reductions of 22.90 and 20.21% at 14 and 28 days in comparison to control. The reduction in FS due to inclusion of NS in CF concrete was ascribed to decreased consistency, leading to fiber agglomeration in the new concrete. This undermines the cement paste, creating many weak paths that promote crack initiation and propagation, ultimately resulting in diminished FS.

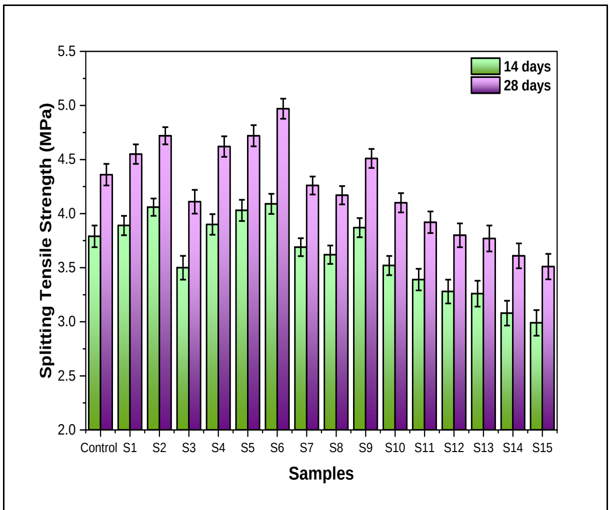

Fig. 8: Split tensile strength results

3.4 Analysis of Split tensile strength (STS)

Fig. 8 illustrates the findings of STS for CFRC. The incorporation of upto 4% CF resulted in an enhancement of STS across all durations. Mix S1 has enhanced STS of approximately 2.64, and 4.36% at 14 and 28 days. Similarly, S2 has superior TS at 14 and 28 days, exceeding the control by 7.12, and 8.26% respectively. The enhancement in STS with incorporation of CF may be attributed to the augmentation of energy transfer mechanism and crack bridging effect facilitated by fiber, which bolstered post-crack failure resistance and elevated STS.

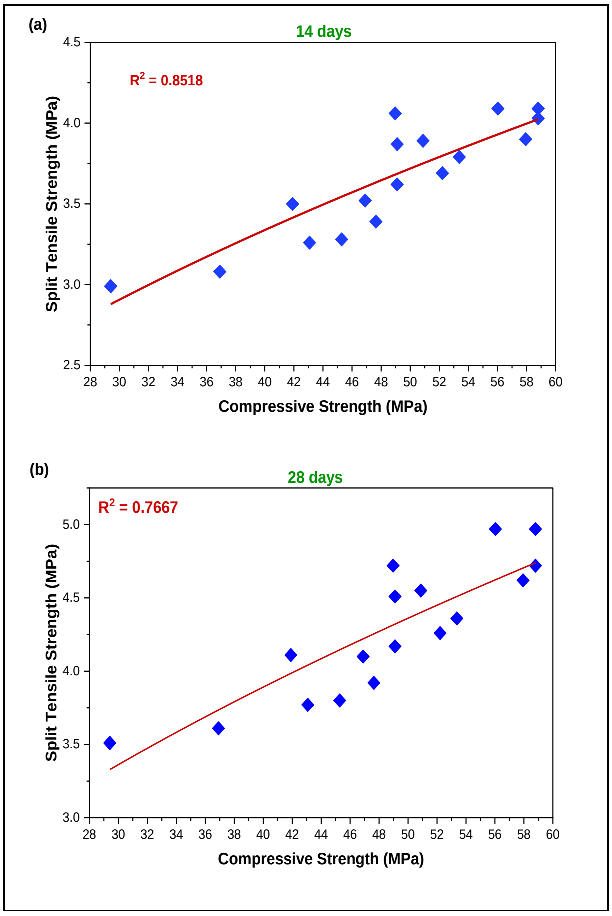

Fig. 9: Correlation between CS and STS of CFRC

The incorporation of 2% NS into plain concrete (lacking CF) enhanced its STS. The tensile strength of S4 exceeded that of the control by 2.90, and 5.96% at 14 and 28 days. The enhancement in STS may result from the reduction in air voids and pore volume within the microstructure of the concrete, attributed to filler properties of NS. This consequently resulted in enhanced adhesion between the aggregate and cement matrix, thereby improving STS. The incorporation of 4% NS to the concrete containing 2 and 4% CF resulted in an enhancement of STS. S5 exhibits enhanced STS of 6.33, and 8.26% compared to the control at 14 and 28 days. Likewise, S6 has enhanced STS by 7.92, and 13.99% at 14 and 28 days, respectively, in comparison to the control. Ultimately, S9 exhibits an enhancement in STS of 2.11, and 3.44% at 14 and 28 days, in relation to the S1. The additional enhancement in STS resulting from the incorporation of NS into the CFRC is attributable to the synergistic effects of both CF and NS. Improved STS was achieved as a consequence of the NS fixing the shortcomings of CF and reinforcing the microstructure of the concrete, which in turn strengthened the link between the fiber and cement. Reduced STS was seen in both CFRC and plain concrete (without CF) upon addition of 4% and 6% NS, respectively. The STS of S8 at 14 and 28 days were lowered by 4.49, and 4.36%, respectively, in contrast to the control. The STS of S12 decreased by 13.46, and 12.84% at 14 and 28 days. An additional decrease is noted with the incorporation of 4% and 6% NS to the CFRC at various CF ratios. At 4 weeks, the STS of S10, S11, S13, S14, and S15 decreased by 5.96, 10.09, 13.53, 17.20, and 19.50%, respectively, relative to the control mix. Previous study shows that, at 91 days, the recycled coarse aggregate mix with CF and ground blast furnace slag had 30.5% higher FS and 33% higher splitting STS than natural-aggregate concrete (Alomayri *et al*. 2023). Because of this, fiber balling effects occurred, and the fibers were not adequately compacted and distributed.

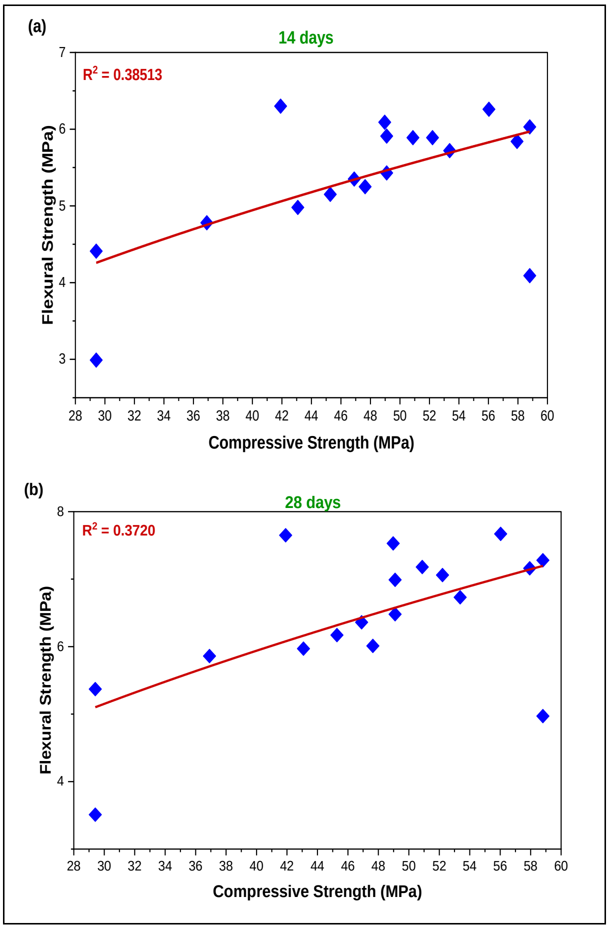

Fig. 10: Correlation among CS and FS of CFRC

3.5 Correlation between CS and STS / FS

Fig. 9 demonstrates the link between CS and STS of CFRC with various proportions of CF and NS, whereas Fig. 10 exhibits the connection between compressive strength and flexural strength. A significant connection is observed between the CS and FS of the concrete at 2 and 4 weeks with R^2 values of 0.3 or above; the correlation at 28 days is the most robust. The STS and FS are accurately correlated with its relevant CS.

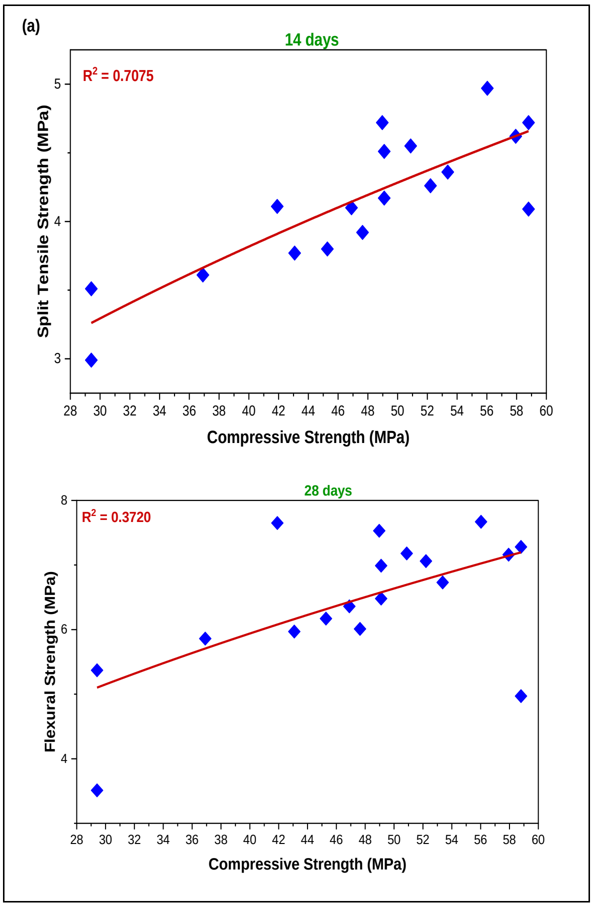

Fig. 11: Power relationship between CS and STS/FS

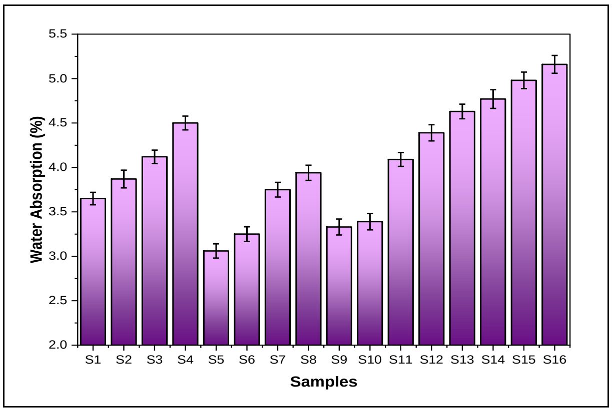

Fig. 12: Water absorption results

All strength relationships display remarkable correlations, with the models for CS *vs* STS and CS *vs* FS exhibiting R^2 values over 0.70 and 0.30. The power model outperforms (Fig. 11) the other models shown in

Fig. 9 and 10 when it comes to forecasting the STS and FS of CFRC based on its CS.

3.6 Water Absorption (WA)

The WA values of S1, S2, and S3 exceeded that of the control by 6.03, 12.88, and 23.29%, respectively (Fig. 12). The augmentation in WA was ascribed to the hydrophilicity of CF due to their elevated lignocellulose content, facilitating water absorption during mixing. Once the concrete cures, it results in surplus pores inside the solidified cement paste, hence enhancing absorption. The ordinary concrete, which lacked CF, experienced a decrease in its WA as a result of the addition of up to 4% NS. In comparison to the control, the WA values of S4 and S8 decreased by 16.16 and 8.77%, respectively. By comparing with previous study, *Agave salmiana* leaves were used as a total additional for calcareous aggregates in plant-based concrete. The hornification process decreased water absorption by 15.2% (Rosas-Díaz *et al.* 2022). The cement matrix densification by nano-silica particles is the cause of decrease in WA. In a combination that contained exclusively 2% CF, the absorption of water was reduced by the addition of up to 4% NS. The negative impact of a 2% CF addition on the water absorption of CFRC was mitigated by the addition of up to 2% NS. In comparison to the control group, the water absorption values of S5 and S9 decreased by 10.96 and 7.12%, respectively. The integration of NS results in the densification of the microstructure, which in turn reduces the porosity generated by CF incorporation, thereby reducing water absorption. Contrarily, both CFRC and plain concrete (without CF) exhibited enhanced water absorption when more than 4% NS was added. This was because the NS had a negative effect on the fresh CFRC's fluidity and consistency, which made compaction and fiber distribution harder. As a result, the microstructure of the concrete became more porous and air voids were larger. Consequently, the porosity and water absorption both were enhanced for CFRC.

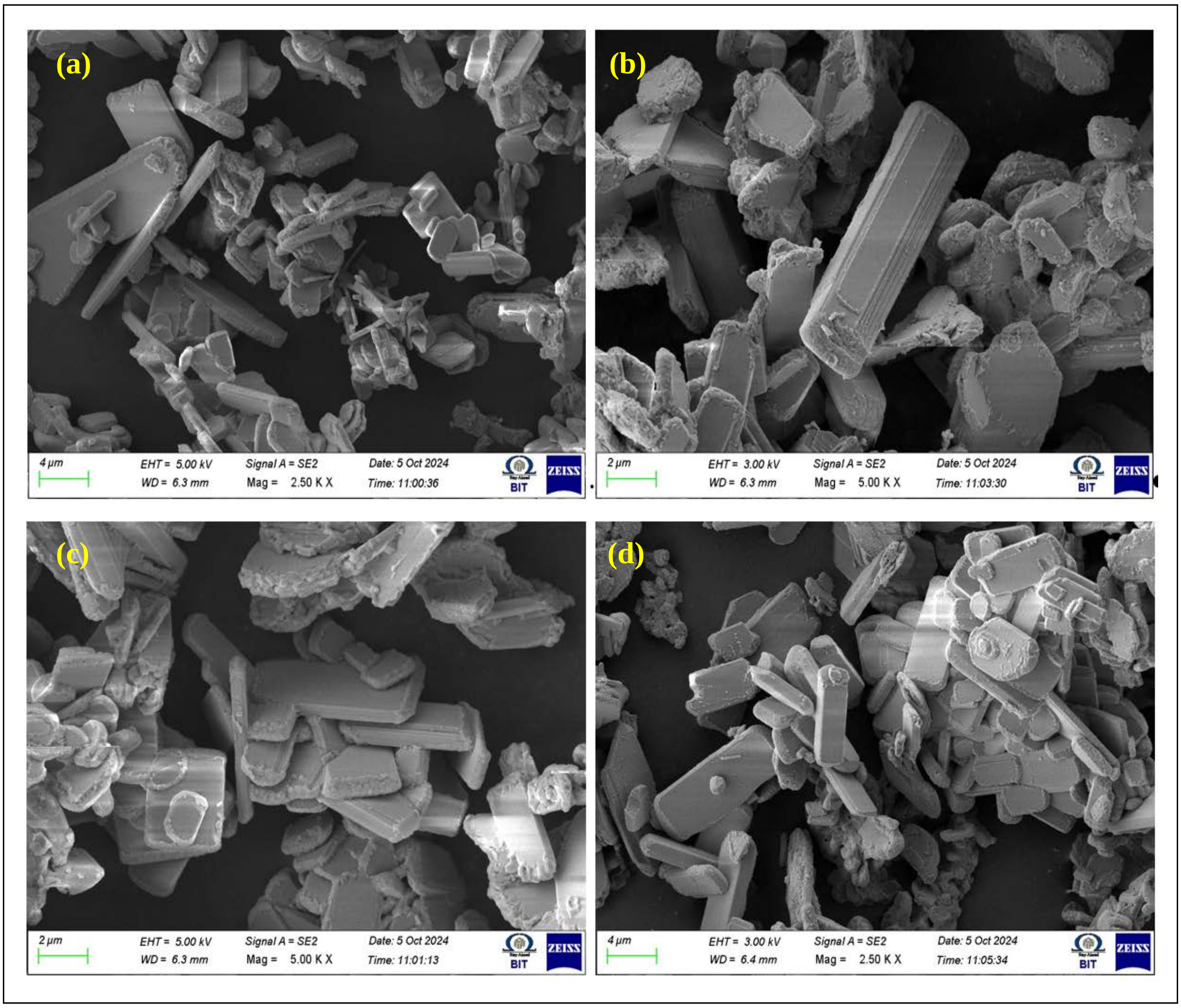

Fig. 13: SEM images of (a) S1, (b) S2, (c) S5, (d) S10 coir fiber reinforced concrete

3.7 Microstructural Analysis

Scanning Electron Microscopy was employed to investigate the influence of CF and NS as additives on the microstructural characteristics of CFRC. The microstructural morphologies of the control mix and numerous combinations that incorporate CF and NS are depicted in Fig. 13. Fig. 13a illustrates that the microstructure is comparatively densified as a result of cement hydration, as evidenced by the scattered fissures and microcracks that are visible on the surface of the concrete mix. The dispersed pores in the microstructure of the control may be the result of air bubbles that are entrapped during mixing, which subsequently dry and create cavities in the matrix. The microstructural morphology of S2 is characterized by the highest porosity and the lowest density, as illustrated in Fig. 13b. This is the consequence of the hydrophilic properties of CF, which result in water absorption during mixture and air entrapment on its surface, which have detrimental effects.

The incorporation of NS into the CFRC enhanced its microstructure and occupied excess pores by CF. The microstructure of S5 is compact, as illustrated in Fig. 13c, followed by S10. Furthermore, a comparison of Fig. 13b and 13d, both of which contain 4% CF, demonstrates that latter's microstructure is more homogeneous and densified, with few apertures than former. Durability assessments in acidic solutions and scanning electron microscopy examination validate that glass fibers and silica fume substantially enhance the concrete's microstructure and performance (Justin *et al*. 2025).

3.8 Optimized results using MEREC – ARAS

The MCDM analysis results yield a detailed rating of the composite formulations according to their mechanical and tribological characteristics. The ideal formulation is determined by balancing various factors, with superior rankings reflecting enhanced overall performance. Table 4 shows the experimental results of Density, Water absorption, Split tensile strength, Flexural strength and Compressive strength.

Table 4. Experimental results for density, water absorption, split tensile, flexural and compressive strength

S. No.	Slump (mm)	Density	STS		FS		CS		WA
			14	28	14	28	14	28	
Control	88	2382	3.79	4.36	5.72	6.73	43.32	53.37	3.65
1	87	2340	3.89	4.55	5.89	7.18	40.83	50.88	3.87
2	84	2295	4.06	4.72	6.09	7.53	39.21	48.97	4.12
3	82	2417	3.5	4.11	6.3	7.65	32.44	41.91	4.5
4	84	2472	3.9	4.62	5.84	7.16	46.85	57.94	3.06
5	83	2396	4.03	4.72	6.03	7.28	48.76	58.8	3.25
6	78	2349	4.09	4.97	6.26	7.67	45.09	56.03	3.75
7	73	2456	3.69	4.26	5.89	7.06	40.52	52.21	3.94
8	69	2483	3.62	4.17	5.43	6.48	39.65	49.1	3.33
9	68	2367	3.87	4.51	5.91	6.99	37.59	49.1	3.39
10	65	2346	3.52	4.1	5.35	6.36	35.39	46.9	4.09
11	65	2317	3.39	3.92	5.25	6.01	33.77	47.64	4.39
12	59	2293	3.28	3.8	5.15	6.17	33.77	45.28	4.63
13	58	2271	3.26	3.77	4.98	5.97	29.79	43.08	4.77
14	56	2246	3.08	3.61	4.78	5.86	29.21	36.91	4.98
15	55	2257	2.99	3.51	4.41	5.37	22.29	29.41	5.16

Table 5. Weight of each alternative for MEREC and ARAS Optimization

Weight	Slump	Densities	Split Tensile Strength		Flexural Strength		Compressive Strength		Water Absorption
			14-day	28-day	14-day	28-day	14-day	28-day	
Aj	0.3188	0.0650	0.2600	0.2519	0.3228	0.3054	0.7084	0.6756	0.3509
Ki	3.2590	-	-	-	-	-	-	-	-
wj	0.098	0.0200	0.080	0.077	0.099	0.094	0.217	0.207	0.108

Table 6. Normalized decision matrix for MEREC – ARAS Optimization

S. No.	Slump	Density	STS		FS		CS		WA
			14	28	14	28	14	28	
1	0.0462	0.0593	0.0611	0.0600	0.0598	0.0585	0.0669	0.0646	0.0627
2	0.0468	0.0583	0.0627	0.0626	0.0616	0.0624	0.0631	0.0616	0.0592
3	0.0484	0.0571	0.0654	0.0650	0.0637	0.0654	0.0606	0.0593	0.0556
4	0.0496	0.0602	0.0564	0.0566	0.0659	0.0664	0.0501	0.0507	0.0509
5	0.0484	0.0615	0.0629	0.0636	0.0611	0.0622	0.0724	0.0701	0.0748
6	0.0490	0.0596	0.0649	0.0650	0.0631	0.0632	0.0753	0.0712	0.0705
7	0.0522	0.0585	0.0659	0.0684	0.0655	0.0666	0.0697	0.0678	0.0611
8	0.0557	0.0611	0.0595	0.0586	0.0616	0.0613	0.0626	0.0632	0.0581
9	0.0590	0.0618	0.0583	0.0574	0.0568	0.0563	0.0613	0.0594	0.0688
10	0.0598	0.0589	0.0624	0.0621	0.0618	0.0607	0.0581	0.0594	0.0676
11	0.0626	0.0584	0.0567	0.0564	0.0560	0.0552	0.0547	0.0568	0.0560
12	0.0626	0.0577	0.0546	0.0539	0.0549	0.0522	0.0522	0.0577	0.0522
13	0.0690	0.0571	0.0529	0.0523	0.0539	0.0536	0.0522	0.0548	0.0495
14	0.0701	0.0565	0.0525	0.0519	0.0521	0.0518	0.0460	0.0521	0.0480
15	0.0726	0.0559	0.0496	0.0497	0.0500	0.0509	0.0451	0.0447	0.0460
16	0.0740	0.0562	0.0482	0.0483	0.0461	0.0466	0.0344	0.0356	0.0444
Optimum	0.0740	0.0618	0.0659	0.0684	0.0659	0.0666	0.0753	0.0712	0.0748
Wj	0.098	0.020	0.080	0.077	0.099	0.094	0.217	0.207	0.108

Table 7. Weighted normalized decision matrix and utility degree rankings

S. No	Slump	Density	STS		FS		CS		WA	Utility degree (Ki)	Rank
			14	28	14	28	14	28			
1	0.00452	0.00118	0.00487	0.00464	0.00593	0.00548	0.01455	0.01339	0.00676	-	-
2	0.00457	0.00116	0.00500	0.00484	0.00610	0.00584	0.01371	0.01276	0.00637	0.86394	4
3	0.00474	0.00114	0.00522	0.00502	0.00631	0.00613	0.01317	0.01229	0.00599	0.85069	7
4	0.00485	0.00120	0.00450	0.00437	0.00653	0.00623	0.01089	0.01051	0.00548	0.84537	9
5	0.00474	0.00123	0.00502	0.00491	0.00605	0.00583	0.01573	0.01454	0.00806	0.7689	12
6	0.00480	0.00119	0.00518	0.00502	0.00625	0.00593	0.01638	0.01475	0.00759	0.93139	2
7	0.00510	0.00117	0.00526	0.00529	0.00649	0.00624	0.01514	0.01406	0.00658	0.94511	1
8	0.00545	0.00122	0.00475	0.00453	0.00610	0.00575	0.01361	0.01310	0.00626	0.92036	3
9	0.00577	0.00123	0.00466	0.00444	0.00563	0.00527	0.01332	0.01232	0.00740	0.85615	6
10	0.00585	0.00118	0.00498	0.00480	0.00612	0.00569	0.01262	0.01232	0.00727	0.84585	8
11	0.00612	0.00117	0.00453	0.00436	0.00554	0.00518	0.01189	0.01177	0.00603	0.85713	5
12	0.00612	0.00115	0.00436	0.00417	0.00544	0.00489	0.01134	0.01195	0.00562	0.79717	10
13	0.00675	0.00114	0.00422	0.00404	0.00534	0.00502	0.01134	0.01136	0.00533	0.77558	11
14	0.00686	0.00113	0.00419	0.00401	0.00516	0.00486	0.01000	0.01081	0.00517	0.76833	13
15	0.00711	0.00112	0.00396	0.00384	0.00495	0.00477	0.00981	0.00926	0.00495	0.73541	14
16	0.00724	0.00112	0.00384	0.00373	0.00457	0.00437	0.00749	0.00738	0.00478	0.70122	15
*	0.00724	0.00123	0.00526	0.00529	0.00653	0.00624	0.01638	0.01475	0.00806		

*Optimum

This study employed MEREC methods on the decision matrix presented in Table 3 to determine the weights of each criterion. The weights derived from the three approaches were subsequently integrated using Equation (6). Table 5 presents the weights from the three approaches beside the total weights. The objective of the optimization approach was to enhance the empirically measured responses, including density, STS (14 and 28 days), FS (14 and 28 days), and CS (14 and 28 days), while minimizing the experimental responses of slump and water absorption.

The ARAS optimizations targeting certain response levels were executed. Each criterion was allocated a goal value weight of (0.098, 0.020, 0.080, 0.077, 0.099, 0.094, 0.217, 0.207 and 0.108), according to the relative importance of each variable to the designated target value. The optimality function outcomes for each alternative option were computed. The normalized choice matrix was constructed using experimental data according to Equation (7 and 8), and the calculated weighted normalized values derived from Equation (9) are displayed in Tables 6 and 7. The utility degree was calculated using Equation (12) and is displayed in Table 7.

The MCDM analysis findings were assessed to identify the ideal concrete mix design by evaluating several performance parameters. The rankings derived from the ARAS optimization method shown a significant correlation with experimental results, underscoring the efficacy of the employed decision-making strategy. The analysis demonstrated that the chosen mixtures attained an optimal equilibrium among mechanical strength, workability, and water absorption. The optimal values were observed at a slump of 78 mm, a density of 2349 kg/m³, split tensile strength of 4.09 MPa at 14 days and 4.97 MPa at 28 days, flexural strength of 6.26 MPa at 14 days and 7.67 MPa at 28 days, compressive strength of 45.09 MPa at 14 days and 56.03 MPa at 28 days, and a water absorption rate of 3.75%. The findings suggest that the best mixtures are suitable for real-time applications in sustainable building, especially in infrastructure projects that necessitate environmentally benign and economical materials. The MCDM technique offered a dependable and impartial framework for identifying the best appropriate concrete mix for certain purposes.

4. CONCLUSIONS

This study investigated the effects of CF and NS on the fresh and hardened properties of CFRC. The incorporation of CF and NS into CFRC resulted in reduced workability, as indicated by the slump test, thereby diminishing the concrete's consistency. The addition of CF led to a reduction in density in both fresh and hardened conditions, whereas incorporating up to 4% NS by cement weight enhanced the density. The compressive strength of CFRC decreased at all ages with the inclusion of CF, with the decline becoming more pronounced as CF concentration increased. However, the incorporation of 2% NS by cement weight improved compressive strength regardless of CF presence and effectively mitigated the strength reduction observed in CFRC with 4% fiber volume. The inclusion of up to 4% CF enhanced the flexural strength (FS) and split tensile strength (STS) of CFRC, while 2% NS further improved these properties and alleviated the decline in tensile and flexural strengths caused by the inclusion of 6% CF. The water absorption (WA) rate increased with higher CF content, but the addition of up to 4% NS reduced WA. Moreover, the incorporation of 4% NS refined the CFRC microstructure by reducing voids created by CF. Finally, multivariable statistical models developed to evaluate the mechanical behavior of CFRC demonstrated exceptional precision and high significance.

FUNDING

This research received no specific grant from any funding agency in the public, commercial, or not-for-profit sectors.

CONFLICTS OF INTEREST

The authors declare that there is no conflict of interest.

5. REFERENCES

Ali, B., Farooq, M. A., El Ouni, M. H., Azab, M. and Elhag, A.B., The combined effect of coir and superplasticizer on the fresh, mechanical, and long-term durability properties of recycled aggregate concrete, *J. Build. Eng.*, 59(2022). https://doi.org/10.1016/j.jobe.2022.105009

Alomayri, T., Yosri, A. M., Ali, B., Raza, S. S., Yaqub, M., Kurda, R. and Deifalla, A.F., The influence of coconut fibres and ground steel slag on strength and durability properties of recycled aggregate concrete: sustainable design of fibre reinforced concrete, *JMR&T.*, 2410027–10039 (2023). https://doi.org/10.1016/j.jmrt.2023.05.212

Balreddy, M. S., Nethra, P. and Naganna, S. R., Performance Evaluation of Open-Graded Bituminous Concrete Modified with Natural Fibers, *Sustainability*, 15(15), 11952(2023). https://doi.org/10.3390/su151511952

Bothiraj, T., Boopathi, K., Kalaiselvan, K., Benham, A. and Mayakannan, S., Experimental investigations on mechanical and wear behavior of waste marble dust and coconut fiber reinforced hybrid bio composites, *Mater. Today Proc*., 2239-2242 (2022). https://doi.org/10.1016/j.Matpr.2022.08.441

Brasil, C. D. S. W., Barroso, S. H. D. A., Picado-Santos, D. L. G., Cabral, A. E. B. and Stefanutti, R., Potential application of by-products from the construction industry and waste from coconuts for concrete road paving blocks: physical and mechanical properties, *Int. J. Pavement Eng.*, 25(1), (2024). https://doi.org/10.1080/10298436.2024.2424392

Bui, H., Boutouil, M., Sebaibi, N. and Levacher, D., Hydration characteristics of coconut fibre-reinforced mortars containing CSA and Portland cement, *J. Mater. Cycles Waste Manag*., 24(4), 1295-1303(2022). https://doi.org/10.1007/s10163-022-01401-0

Crucho, J., Picado-Santos, L. and Neves, J., Cement-treated pavement layers incorporating construction and demolition waste and coconut fibres: a review, *J. Mater. Cycles Waste Manag*., 23(14), 4877-4896(2022). https://doi.org/10.1080/10298436.2021.1984475

Dora, S., Barta, R. B. and Mini, K. M., Study on foam concrete incorporated with expanded vermiculite/capric acid PCM – A novel thermal storage high-performance building material, *Constr. Build Mater*., 392(2023). https://doi.org/10.1016/j.conbuildmat.2023.131903

Gupta, R. K., Mayakannan, S., Vijayaraghavalu, S., Poornima, M. M., Nanthakumar, S. and Bhaskaran, N. A., Multi-objective Optimization of Bamboo-madar Fiber Reinforced Composites for Lightweight Automotive Applications using Machine Learning and Genetic Algorithms, *J. Environ. Nanotechnol*., 13(4), 358–376(2024). https://doi.org/10.13074/jent.2024.12.244978

Hameed, S., Gillani, S. A. A., Tahir, M., Hameed, R., Abbas, S., Nehdi, M. L. and Ahmad, M., Investigating lightweight recycled brick aggregate concrete incorporating EPS beads: Application to masonry units, *RINENG*., 25(2025). https://doi.org/10.1016/j.rineng.2025.104019

James, J. S. and John, E., Synergistic effects of SCMs and fibers on plastic shrinkage control of sustainable concrete, *Green Mater*., 1-17(2025) https://doi.org/10.1680/jgrma.24.00169

Justin, S., Thushanthan, K. and Tharmarajah, G., Durability and mechanical performance of glass and natural fiber-reinforced concrete in acidic environments, *Constr. Build Mater*., 465(2025). https://doi.org/10.1016/j.conbuildmat.2025.140262

Kandasamy, S., Ilangovan, P., Kanagaraj, R., Sellamuthu, M. and Karunakaran, A., Effect of sisal and coconut fibers on the strength performance of recycled aggregate concrete using copper slag, *Int. J. Adv. Manuf. Technol.*, 130(1–2), 731–737(2024). https://doi.org/10.1007/s00170-023-12695-1

Menon, A. R., Konnur, S. and Bhasi, A., Model Tests on Coir Geotextile-Encased Stone Columns with Tyre Crumb-Infilled Basal Coir Geocell, *Int. J. of Geosynth. and Ground Eng*., 7(2), 38(2021). https://doi.org/10.1007/s40891-021-00274-x

Odeyemi, S. O., Adisa, M. O., Atoyebi, O. D., Adesina, A., Ahmed, L. and Adeniyi, O.I., Variability Analysis of Compressive and Flexural Performance of Coconut Fibre Reinforced Self-Compacting Concrete, *JERA*., 66, 19–27(2023). https://doi.org/10.4028/p-kcF6YL

Özkılıç', Y. O., Beskopylny, A. N., Stel'makh, S. A., Shcherban', E. M., Mailyan, L. R., Meskhi, B., Chernil'nik, A., Ananova, O., Aksoylu, C. and Madenci, E., Lightweight expanded-clay fiber concrete with improved characteristics reinforced with short natural fibers, *Case Stud. Constr. Mater*., 19(2023). https://doi.org/10.1016/j.cscm.2023.e02367

Rajkohila. A., Chandar, S. P. and Ravichandran, P. T., Flexural Performance of HSC beams containing natural fibers, *J. Build Rehabil.*, 9(71), (2024). https://doi.org/10.1007/s41024-024-00423-5

Sathishkumar, P., Chebolu, S. R., Giri, R., Sathish, J. T. and Fatehmulla, A., Impact of different parameters in tribological properties of enset ventricosum/ terminalia arjuna fibers/SiO_2 filler incorporation, *J. Mater. Res. Technol*., 33, 3826-3836(2024). https://doi.org/10.1016/j.jmrt.2024.09.250

Pederneiras, C. M., Veiga, R. and de Brito, J., Physical and mechanical performance of coir fiber-reinforced rendering mortars, *Materials*, 14(4), 1–15(2021). https://doi.org/10.3390/ma14040823

Poongodi, K., Murthi, P. and Revathi, P., Influence of coir fibre and recycled aggregate on bond strength of pavement quality concrete, *Mater. Today Proc*., 61, 400–405(2022). https://doi.org/10.1016/j.matpr.2021.10.370

Rahmawati, C., Handayani, L., Faisal, M., Zardi, M., Sapuan, S. M., Hadi, A. E., Ahmad, J. and Isleem, H.F., Optimization of Mortar Compressive Strength Prepared with Waste Glass Aggregate and Coir Fiber Addition Using Response Surface Methodology, *J. Renew Mater*., 11(10), 3751–3767(2023). https://doi.org/10.32604/jrm.2023.028987

Rosas-Díaz, F., García-Hernández, D. G., Mendoza-Rangel, J. M., Terán-Torres, B. T., Galindo-Rodríguez, S. A. and Juárez-Alvarado, C. A., Development of a Portland Cement-Based Material with *Agave salmiana* Leaves Bioaggregate, *Materials*, 15(17), 6000(2022). https://doi.org/10.3390/ma15176000

Samson, A. O., Antoinette, G. O., Tobit, I. U. and Ibukunoluwa, S.D., Impact resistance and durability of natural fibre reinforced concrete pavement and partial replacement with steel slag aggregate, *J. Mater. Cycles Waste Manag*., 26(2), 936–945(2024). https://doi.org/10.1007/s10163-023-01871-w

Senguttuvan, K., Natarajan, S., Govindan, D.C. and Easwaran, S.K., Impact of inclusion of lignocellulosic fibre, metal swarf and industriawaste by products to develop sustainable environment, *Matéria (Rio J.)*, 29(3), e20240030(2024). https://doi.org/10.1590/1517-7076-RMAT-2024-0030

Sharma, R. and Senthil, K., Reviewing on influence of waste materials on structural concrete under impact loading, *IJSTRUCTE*., 12(2), 103–124(2022). https://doi.org/10.1504/IJSTRUCTE.2022.121985

Padmakumar, V., G. and Madhavan, M. K., Experimental Investigation on Performance of Fiber-Reinforced Foam Concrete Incorporated with Vermiculite, *J. Mater. Civ. Eng*., 35(11), (2023). https://doi.org/10.1061/JMCEE7.MTENG-15460

Waqar, A., Bheel, N., Almujibah, H. R., Benjeddou, O., Alwetaishi, M., Ahmad, M. and Sabri, M. M. S., Effect of Coir Fibre Ash (CFA) on the strengths, modulus of elasticity and embodied carbon of concrete using response surface methodology (RSM) and optimization, *RINENG*., 17(2023). https://doi.org/10.1016/j.rineng.2023.100883

Zhang, X., Pel, L., Gauvin, F. and Smeulders, D., Reinforcing mechanisms of coir fibers in light-weight aggregate concrete, *Materials*, 14(3), 1-20(2021). https://doi.org/10.3390/ma14030699